Electronic Supplementary Information

Nanocellulose/Bioactive Glass Cryogels as Scaffolds for Bone Regeneration

Filipe V. Ferreira[a,b,c,d*], Lucas P. Souza[e], Thais M.M. Martins[f], João H. Lopes[g], Bruno D. Mattos[c], Marcos Mariano[b], Ivanei F. Pinheiro[a,b], Thalita M. Valverde[h], Sébastien Livi[d], José A. Camilli[e], Alfredo M. Goes[h], Rubia F. Gouveia[b], Liliane M.F. Lona[a], Orlando J. Rojas[c*]

a. School of Chemical Engineering, University of Campinas (UNICAMP), 13083-970, Campinas-SP, Brazil.

b. Brazilian Nanotechnology National Laboratory (LNNano), Brazilian Center for Research in Energy and Materials (CNPEM), 13083-970, Campinas-SP, Brazil.

c. Department of Bioproducts and Biosystrems, Aalto University School of Chemical Engineering, P.O. Box 16300, 00076, Aalto University, Finland.

d. Université de Lyon, Ingénierie des Matériaux Polymères CNRS, UMR 5223, INSA Lyon, F-69621 Villeurbanne, France.

e. Department of Structural and Functional Biology, Institute of Biology, University of Campinas (UNICAMP), 13083-862, Campinas-SP, Brazil.

f. Department of Morphology, Institute of Biological Sciences, Federal University of Minas Gerais (UFMG), 31270 -901, Belo Horizonte-MG, Brazil.

g. Department of Chemistry, Division of Fundamental Sciences (IEF), Technological Institute of Aeronautics (ITA), 12228-900, Sao Jose dos Campos-SP, Brazil.

h. Department of Biochemistry and Immunology, Institute of Biological Sciences, Federal University of Minas Gerais (UFMG), 31270 -901, Belo Horizonte-MG, Brazil.

Table of Content

SECTION 1 – Materials

An aqueous suspension (3% solids) of cellulose nanofibrils (CNF) from *Eucalyptus grandis* was kindly supplied by Suzano Papel e Celulose SA (Brazil). All precursors reagents used for the bioactive glass synthesis were purchased from Sigma-Aldrich (St. Louis, MO, USA). High purity silicon dioxide (SiO_2), sodium carbonate (Na_2CO_3), calcium carbonate ($CaCO_3$), and phosphorus pentoxide (P_2O_5) powders (> 99.9%) were obtained from Sigma-Aldrich.

SECTION 2 - Preparation of bioactive glass and cryogels

Bioglass preparation.

Thirty-gram batches of 46.1 mol.% SiO_2, 26.9 mol.% CaO, 24.4 mol.% Na_2O, and 2.6 mol.% P_2O_5 were melted in a platinum crucible at 1400 °C in air for 3 h using a furnace (Lindberg/Blue M 1700 °C, Thermo Electron Corporation, Asheville, NC, USA). Then, the melt was quenched in air within graphite molds, annealed at 500 °C, and slowly cooled down to room temperature for 12 h in order to relief the thermal stress.

Composite cryogel preparation

Different amounts of bioactive glass were first dispersed in deionized water using bath ultrasonication (5 min, room temperature). The dispersion containing bioactive glass was then added to the CNF suspension and the mixture was magnetically stirred for 5 min to ensure homogeneous dispersion. The bioactive glass content was controlled in order to obtain composite cryogels with 60, 75, and 80 wt.% of bioactive glass. The samples were prepared and poured into cylindrical polypropylene molds, frozen at -20 °C for 24 h, and lyophilized to remove ice by sublimation. Neat CNF cryogels (Pure CC) were prepared following the same procedure, except for the absence of bioactive glass, and used as reference. Composite cryogels containing 60, 75, and 80 wt.% of bioactive glass were labeled CC-Bio1, CC-Bio2, and CC-Bio3, respectively. Pure CC (control) and CC-Bio3 (cryogel featuring the best mechanical performance) were selected for bioactivity assessment through hydroxyapatite formation, as well as *in vitro* and *in vivo* performances as scaffolds. Pure CC and CC-Bio3 are thereafter referred to as CC and CC-Bio, respectively.

SECTION 3 - Characterization

Atomic force microscopy (AFM)

AFM images were obtained on a NX-10 atomic force microscope (Park System) operating on intermittent contact. One drop (7 μL) of CNF suspension (0.001 wt.%) was deposited onto freshly cleaned mica and dried under ambient atmosphere for 24 h. Fiber diameter was obtained through the Z-axis (height) of topography images. More than150 fibers were analyzed per treatment and the result is expressed as mean ± standard deviation (SD) values.

Thermogravimetric analysis (TGA)

The thermal degradation profile of the cryogels (10-mg samples) were determined in a thermogravimetric analyzer (model TGA 7HT, Perkin Elmer, Waltham, MA, USA) under an air flow rate of 50 mL min^{-1} at temperatures ranging from 25 to 1000 °C at a constant heating rate of 10 °C min^{-1}.

Uniaxial compression test

Mechanical resistance of the cryogels was studied by compression test using a universal testing machine (model DL2000, EMIC Equipamentos e Sistemas de Ensaio Ltda., São José dos Pinhais, Brazil) at room conditions. Ten 10-mm-diameter cylindrical monoliths of each composition were compressed at 2 mm min^{-1} using a 50-N static load cell. The compressive modulus was calculated using the first linear part of the curve force *vs* deformation taking into account original sample dimensions. Yield stress and energy absorption were determined at 1% and up to 70% strain, respectively.

Internal structure and porosity

The composite scaffold structure was three-dimensionally reconstructed by high-resolution X-ray micro-computed tomography (Resolution: 1 pixel = 4.5 μm) (μCT; model Skyscan 1272, Bruker microCT, Kontich, Belgium). The projections of the cellulose monoliths were acquired using a current of 175 μA and source voltage of 30 kV. μCT was also used to image the calvaries of rats, being the amount of bone formed within the defect (procedure described below) calculated using a pre-determined volume of interest. The amount of bone found in the control was taken as the blank, which was subtracted from the other values.

Fourier-transform infrared (FTIR) spectroscopy

Short-range ordering in the cryogels before and after dipping in a simulated body fluid (SBF) was characterized in a FTIR spectroscope (model Nicolet 6700, Thermo Electron Co., Waltham, MA, USA) equipped with single reflection ATR. FTIR spectra were acquired in the region 4000-400 cm^{-1} with spectral resolution of 4 cm^{-1} and 64 scans.

Inductively coupled plasma optical emission spectrometry (ICP-OES)

The ionic leaching patterns of the bioactive glass were determined by ICP-OES. Briefly, 300 mg of cellulose cryogels (CC) were immersed in 200 mL buffer solution under continuous stirring (75 rpm) at room temperature during 24 h. The solution pH was adjusted to 7.4 using a 50.69 mM HEPES (2-(4-(2-hydroxyethyl)piperazin-1-yl)ethanesulfonic acid) and 1 mM sodium hydroxide (NaOH). At each time interval (5, 15, 30, 60, 180, 360, 720, and 1440 min), 5-mL solution was collected with a syringe, passed through a 0.22-μm-pore diameter filter (Millipore®), and analyzed in an ICP-OES spectrometer (Optima 8300 ICP-OES, PerkinElmer, Inc., Shelton, CT, USA). The measurements were conducted in triplicate.

X-ray photoelectron spectroscopy (XPS)

The chemical surface of cryogels were analyzed using a K-Alpha X-ray photoelectron spectrometer (Thermo Fisher Scientific, UK) equipped with hemispherical electron analyzer and monochromatic Al Kα (1486.6 eV) radiation. The samples were immersed in simulated body fluid (SBF) during 7 days at 37 °C, and XPS analyzes were carried out before and after immersion. Survey (full-range) and high-resolution spectra for C, Ca, O, P, and Si were acquired and the average of three measurements performed on different regions along the samples was reported.

Scanning electron microscopy (SEM)

The formation of hydroxyapatite on cryogel surface after immersion in complete culture medium was investigated using SEM. The samples were studied using FEG - Quanta 200 FEI operating at 10 kV available at the Center of Microscopy at the Federal University of Minas Gerais.

Mineralization assay

MC3T3-E1 cells were plated at density of 1 x 10^4 cells/in 6-well plates. Once plated, the cells received basal medium supplemented with an osteogenic solution (7 mM β-

glycerophosphate and 5 μg/mL ascorbic acid; Sigma-Aldrich). After allowing cells to adhere, the scaffolds were placed in contact with the cells. After 14 days in osteogenic induction medium, the deposition of a mineralized matrix was assessed by alizarin red staining. The cells were washed with 0.15 M PBS (pH 7.2) and fixed with ethanol (70 vol.%) for 1 h at 4 °C. After fixation, the cells were washed with 0.15 M PBS (pH 7.2) and Milli-Q water. Then, 1 mL of alizarin red dye (2%) was added and the cells were incubated for 15 min at room temperature. The excess of dye was removed and the cells were washed with Milli-Q water. After that, washing with 0.15 M PBS (pH 7.2) was performed for 15 min followed by rapid washing with Milli-Q water and drying at room temperature. Cells were observed under light microscopy (Olympus IX70) and photographed (Olympus Evolt E-300).

Evaluation of the *in vitro* biocompatibility of CC and CC-Bio

In vitro biocompatibility of the cryogels was evaluated with MC3T3-E1 cells by live/dead and MTT viability assay. A murine pre-osteoblastic cell line MC3T3-E1 was obtained from the American Type Culture Collection (Arlington, VA) and cultured in Minimum Essential Medium-α (MEM-α; Gibco, Carlsbad, CA, USA) supplemented with 10% fetal bovine serum (Invitrogen, Carlsbad, CA, USA) and 1% antibiotic/antimycotic solution (Sigma-Aldrich, St. Louis, MO, USA). The cells were maintained at sub confluent densities with 3 weekly medium changes at 37 °C in a humidified atmosphere containing 5% CO_2. At 80–90% confluence, the cells were detached using 0.05% trypsin–EDTA (Gibco, Carlsbad, CA, USA), counted in a Neubauer chamber (HBG, Gießen, Germany), and used to perform the experiments. MC3T3-E1 cells were plated at a density of 1 x 10^4 cells/well in 24-well culture plates. After allowing cells to adhere, the CC and CC-Bio were placed in contact with the cells and incubated at 37 °C, 5% CO_2, and humid atmosphere.

Live/dead viability/cytotoxicity assay was studied as follows: after 72 h of incubation, the cells were washed with PBS and incubated with 5 μM Calcein-AM (Thermo Fisher Scientific, Rockford IL, USA) and 2 μM ethidium bromide (Sigma-Aldrich, St. Louis, MO, USA) for 5 min at 37 °C. After rinsed with PBS, the cells were visualized through fluorescent microscopy (Olympus IX70, Japan) and photographed using the Image Pro Plus 7.01 software. Cell analysis was performed using the Image J software. Staurosporine (200 nM; Sigma-Aldrich) was used as a positive control for cell

death and the cells seeded in 24-well culture plates without the cryogels were used as negative control.

MTT viability assay: at three time points (24, 48, and 72 h), the medium was removed and a solution containing 210 µL of culture medium and 170 µL of MTT (5 mg/mL) was added per well. After 2 h incubation at 37 °C, the supernatant was removed and the formazan crystals were dissolved with acid-isopropanol (0.04 N HCI in isopropanol). After 10 min at room temperature, 100 µL of each well was transferred in triplicate to a 96-well plate and the absorbance was measured at 570 nm and a reference wavelength of 630 nm (Multiskan GO Microplate Spectrophotometer, Thermo Fisher Scientific, Rockford, IL, USA). Cells seeded in 24-well culture plates without the cryogels were used as negative control. The values were expressed as percentages of the negative control. The experiments were performed in biological triplicates. All data were analyzed in GraphPad Prism 6.0 software (San Diego, CA, USA).

Experimental *in vivo* model

In vivo studies were approved by Ethics in Research Committee (CEUA/UNICAMP n° 4647-1/2017) and carried out at the Department of Structural and Functional Biology - Institute of Biology, University of Campinas. Eighteen male, 2-month-old rats (Wistar) were used. A calvarial defect (mini-rolls of 5 mm in diameter) was made to insert the scaffolds. The animals were divided in 3 groups (6 rats/group) according to the treatment applied to the bone defect: group I (control), group II (pure cellulose cryogel, CC), and group III (cryogels containing bioglass, CC-Bio). Along all the experimental time, the rats were kept in standard boxes in controlled environmental conditions (12 h bright/dark cycles) with standard food and water.

Systemic toxicity was studied after eight weeks of surgery. All rats were euthanized and their kidneys, liver, and blood were collected. Organs were histopathologically analyzed. For this, they were fixed with Bouin solution for 24 h and paraplast embedded (Sigma-Aldrich). Histological sections with 5 µm of thickness were stained using Hematoxilyn and Eosin and examined under a light microscope. Systemic toxicity was also investigated by quantifying the serum concentration of biochemical toxicological markers from liver (TGO/TGP) and kidney (Creatinine) using enzymatic kits (Interkit®) and comparing all values with control group.

The serum concentrations of bone morphogenetic protein 2 (BMP-2) were quantitatively determined by ELISA kit (Rat BMP-2 ELISA kit, Elabscience®). Firstly,

blood was centrifuged for 15 min (at 1000xg and at 2~8 °C) and then the supernatant was collected. To guarantee high purity, this procedure was performed twice. After separation, 100 µL of sample or standard were added to each well and incubated at 37 °C for 90 min. Subsequently, the liquid was removed and 100 µL of biotinylated antibody was added to each well and incubated for 1 h at 37 °C. Following the incubation time, all wells were washed 3 times using wash solution and 100 µL of HRP conjugate was added to each well and left at 37 °C for 30 min. Wells were then aspirated and washed 5 times prior to the addition of 90 µL of substrate reagent, which was incubated for 15 min at 37 °C. Stop solution was added and the plate was immediately read at 450 nm.

Statistical analysis

Statistical analyses were performed for the live/dead and MTT viability assay using a one-way analysis of variance (ANOVA) followed by Tukey's post-test. Results with $p < 0.05$ were considered statistically significant. For the *in vivo* assays, statistical analysis of data (n=6) was performed by one-way ANOVA at the same confidence level (95%). All data were expressed as mean ± standard deviation (SD) values.

SECTION 4 - Supporting discussion

Discussion S1: Thermal and mechanical properties of cryogels

The thermogravimetric profiles of pure cellulose cryogel and cryogels containing bioglass are shown in **Figure S1b-c**. A small mass loss at low temperature (<120 °C) was observed for all samples, which is related to the evaporation of water (moisture) physically adsorbed on the cryogel surface, provided the highly hygroscopic nature of cellulose. Interestingly, CC-Bio showed a less pronounced moisture loss when compared to pure CC, suggesting the chemical interaction between the surface groups of bioglass particles (≡Si-OH) and the hydroxyl groups of cellulose, the latter accounting for the high affinity to moisture of neat CNF cryogels. This interaction may reduce the water retention capacity on the CC-Bio surface, decreasing the mass loss due to moisture desorption. The threshold temperature corresponding to the completion of moisture loss occurred at *ca.* 130 °C, thereafter sample surface was composed mainly by dehydrated hydroxyl groups and only strongly bound water molecules (water of hydration). The second thermal event, which occurred within a wide temperature range (269-378 °C) for all samples, was assigned to the thermal degradation of external cellulose chains and volatile materials of cellulose matrix.[1] On the other hand, pure CC and CC-Bio showed different thermal degradation processes during the third event: pure CC showed the highest thermal degradation rate at 474 °C, while in CC-Bio this occurred at about 411 °C. Moreover, this third thermal event decreased as bioactive glass content in the cryogel increased. Probably, greater amount of bioactive glass increases the diffusion of heat to the sample, accelerating the degradation of cellulose inner layers. By normalizing the mass loss data, it is possible to infer that the bioactive glass content in CC-Bio1, CC-Bio2, and CC-Bio3 samples were approximately 60, 74, and 81%, which agree well with the amounts used during the preparation (60, 75, and 80 wt.%, respectively).

The uniaxial compression test (**Figure S1d**) demonstrated that the addition of low amount of bioactive glass (less than 75 wt.%) presented no significant effect on the compressive modulus of the cryogel, whereas the addition of 80 wt.% of bioactive glass significantly improved the compressive modulus of the sample. Moreover, a flexible structure was still observed despite this great amount of bioactive glass (**Figure S1e-f**). The flexible structure of CC-Bio3 did not differ from the structure of pure CC, but it differed from 100% bioactive glass material structure that is very fragile[2]. The results of

yield stress and energy absorption followed the same trend of the compressive modulus. Therefore, the addition of large amounts of bioactive glass led to a material with commensurate flexible properties when compared to those from pure CNF-based cryogel.

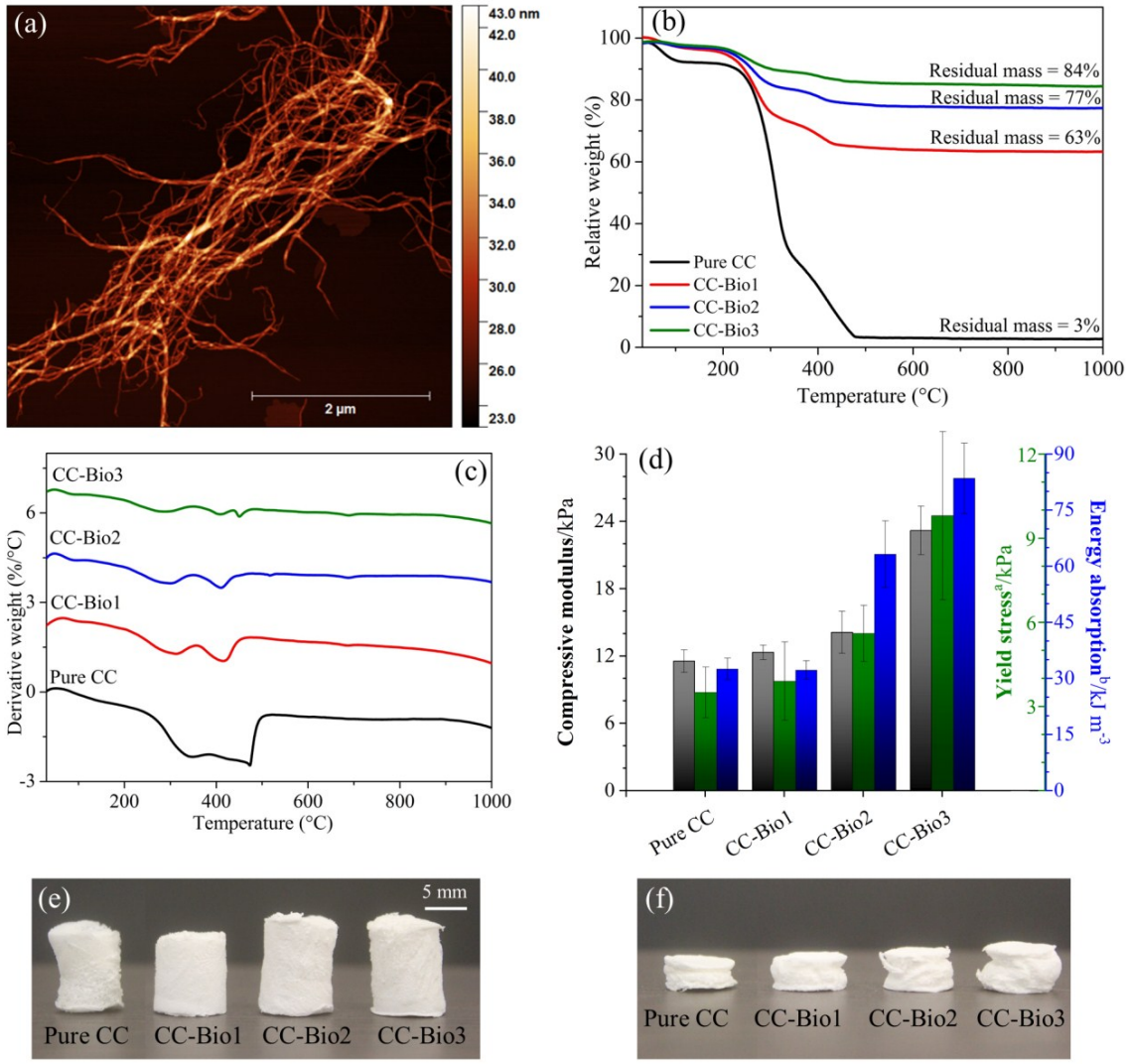

Figure S1. (a) Representative atomic force microscopy image of cellulose nanofibers (CNFs) from *Eucalyptus grandis*; (b) Thermogravimetric (TG) and (c) derivative TG (DTG) curves of pure (Pure CC) and bioactive glass-containing (inorganic load in CC-Bio1 < CC-Bio2 < CC-Bio3) CNF-based cryogels; (d) Compressive modulus, yield stress and energy absorption of pristine and composite CNF-based cryogels (n=10; [a]Yield stress determined at 1% strain; [b]energy absorption up to 70% strain); (e-f) Photographs of the cryogel monoliths (e) before and (f) after mechanical assay, evidencing a non-brittle and flexible behavior under compression.

Discussion S2: Morphology of CNFs and cryogels

The morphological characteristics of the *E. grandis*-derived CNF herein used in cryogel preparation were studied by AFM (**Figure S1a**). A nanofibrillated structure comprising long and flexible fibrils could be clearly identified. These fibrils had 13 ± 6 nm in width (determined by sample height) and a few micrometers in length, therefore featuring aspect ratios greater than 50. Such a high length-to-width value is typical of nanofibrillated cellulose and highly desirable for foam production as it imparts high entanglement levels, which in turn are capable of preventing the collapse of the three-dimensional structure even in the absence of chemical crosslinking[3,4].

Morphological study of the cryogels was performed using X-ray microtomography. The results revealed that structural characteristics of CNF-based cryogels were preserved after addition of bioactive glass (**Figure S2a-h**). All samples showed an interconnected 3D network with high porosity. Moreover, the morphometrical results (**Figure S2i-l**) showed that the cryogel wall thickness increased, while the porosity reduced as the amount of bioactive glass increased. This behavior is probably related to the coating of the cryogel walls and the partial fill of the of the cryogel pores by the bioactive glass during preparation. These results allow us to conclude that the highest value of mechanical properties observed for the CC-Bio3 may have been favored at the expense of decreased porosity. Finally, for comparison, Figure S3, shows SEM micrographs of CC and CC-Bio and the respective pore size histograms according to this method.

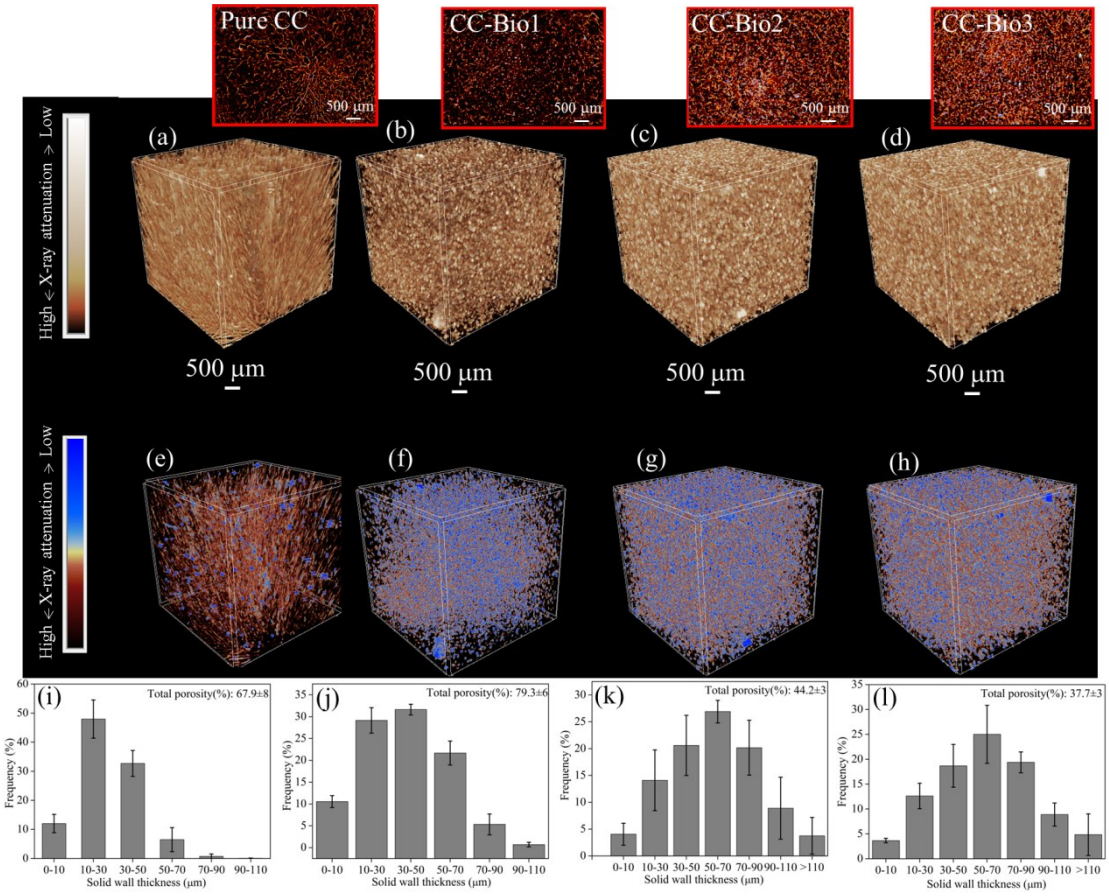

Figure S2. Morphological and morphometric analyses of the cryogels performed by X-ray micro-computed tomography: (a, e and i) Pure CC; (b, f and j) CC-Bio1; (c, g, and k) CC-Bio2 and (d, h and l) CC-Bio3. Figure (a-h) correspond to 3D reconstruction. 2D slice inside the 3D image are shown at the top right corner of figure (a-d). Figure (i-l) correspond to wall thickness and the porosity of the cryogels.

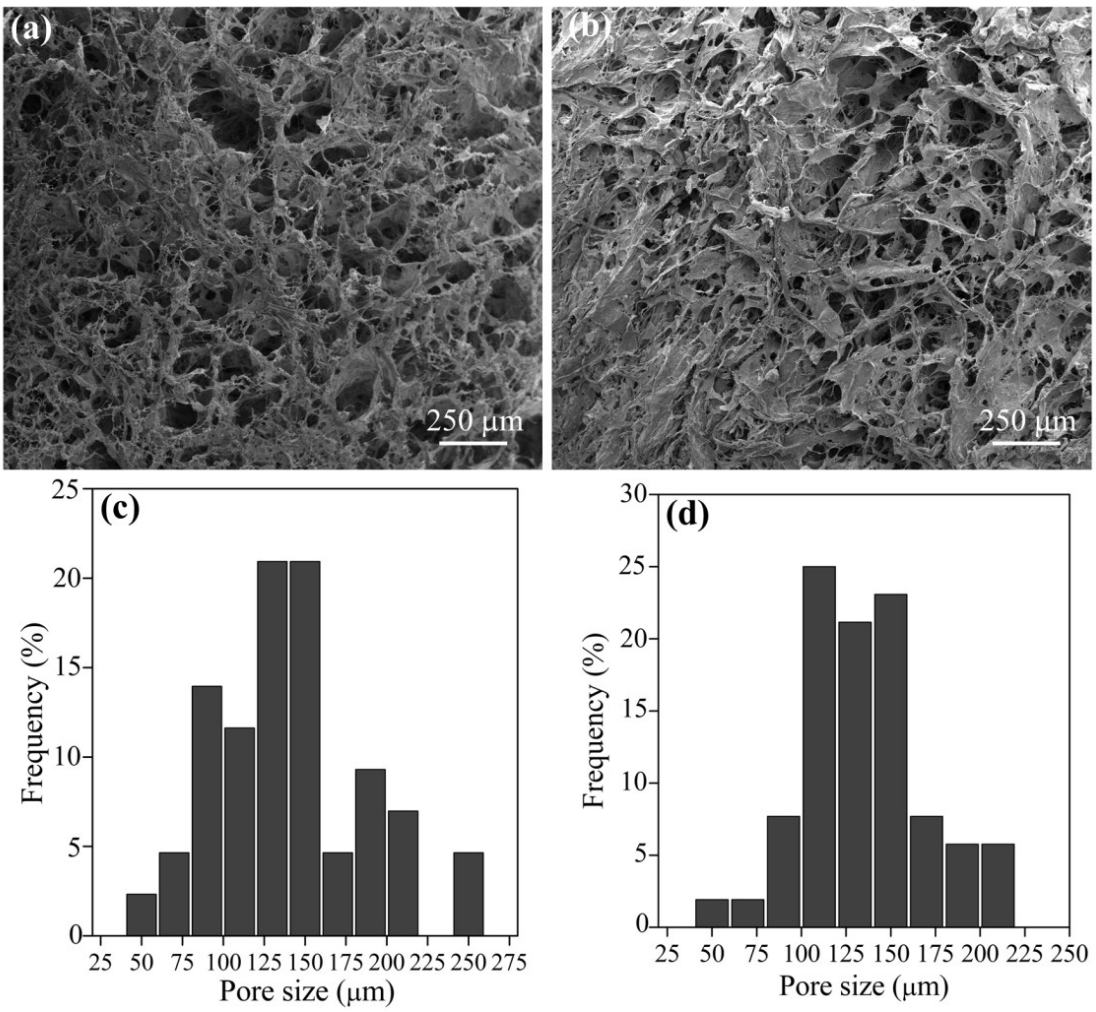

Figure S3. SEM micrographs of (a) CC and (b) CC-Bio. Pore size distribution histogram of (c) CC and (d) CC-Bio.

Discussion S3: Fourier-transform infrared (FTIR) spectroscopy

Insights into the chemical structure and features of CC and CC-Bio were obtained by ATR FTIR spectroscopy (**Figure 2a**). The infrared spectra for the cryogels indicated the typical absorption bands of pure cellulose: a strong absorption at the high frequency range (3600-3000 cm^{-1}) assigned to hydrogen-bonded OH stretching; a band at 2912 cm^{-1} associated with the C-H stretching mode: and an absorption peak at 1640 cm^{-1} related to the deformation mode of undissociated water molecules ($\delta_{H\text{-}O\text{-}H}$).[1] Deformation modes of C-H in the CH_2 and the complex band were observed at intermediate frequencies (1400-1370 cm^{-1}), while the bands associated with the C-O stretching mode of the C-O-C and C-OH groups were observed at 1032, 1055, 1108, 1160 and 1200 cm^{-1}.[1]

As expected, the main differences observed in CC-Bio and pure CC spectra were the signals corresponding to the bioactive glass. In this context, the absorption related to cellulose was superimposed by the bioactive glass signals, the major component in the CC-Bio. The spectrum of CC-Bio showed two absorptions at 1505 and 1433 cm^{-1} associated with the presence of carbonates.[5]

Discussion S4: X-ray photoelectron spectroscopy (XPS)

XPS analysis was performed to better understand the chemical bonding and structures on the surface of CC-Bio. The ability of CC-Bio to form apatite layer in the presence of a SBF was also evaluated. **Figure S4** shows the XPS survey spectra of pure CC and CC-Bio before and after immersion in SBF for 7 days, whereas the element compositions on the surface are summarized in **Table S1**.

Table S1. Surface elemental composition of cellulose nanofiber-based cryogels either added (CC-Bio) or not (Pure CC) by bioactive glass,, determined by X-ray photoelectron spectroscopy either before (no label) or after immersion in simulated body fluid (SBF).

Photopeaks	Composition (at.%)†			
	Cryogels			
	Pure CC	Pure CC in SBF	CC-Bio	CC-Bio in SBF
C_{1s}	54.7	56.9	42.2	27.9
O_{1s}	41.9	33.0	45.4	44.4
Si_{2p}	1.5	–	3.1	2.0
Ca_{2p}	0.5	0.9	2.6	8.9
P_{2p}	–	1.0	0.7	5.6
N_{1s}	0.6	2.7	–	1.3
Cl_{2p}	–	3.2	0.4	5.8
Na_{1s}	0.8	2.3	5.6	3.0
Mg_{1s}	–	–	–	0.9

†Surface composition was obtained by survey XPS spectra. The concentrations of C, O, Si, Ca, P, N, Cl, Mg, and Na were acquired by the signals of C_{1s}, O_{1s}, Si_{2p}, Ca_{2p}, P_{2p}, N_{1s}, Cl_{2p}, Na_{1s}, and Mg_{1s}, respectively.

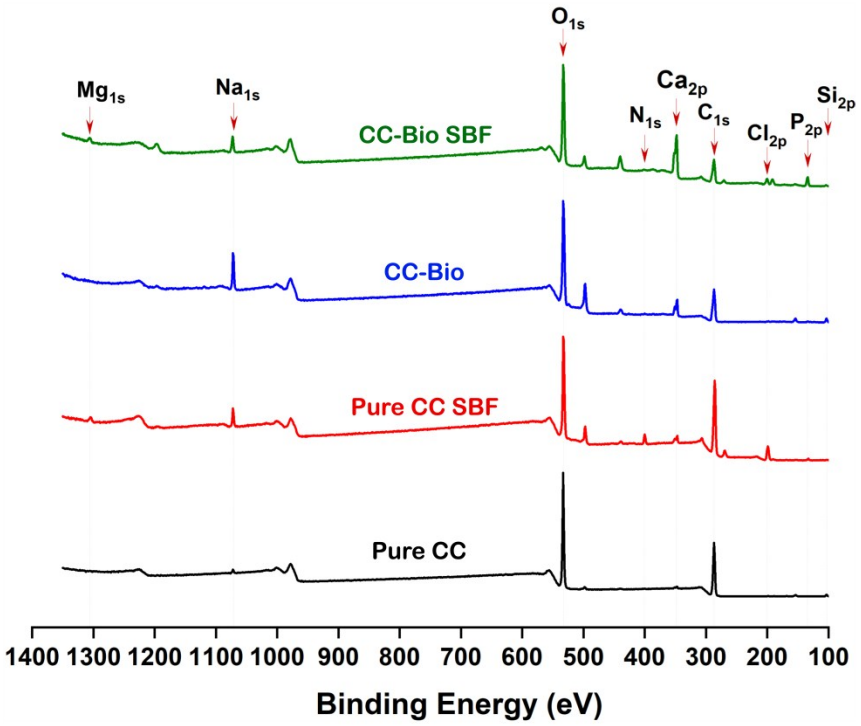

Figure S4. Survey X-ray photoelectron spectra of CNF-based cryogels either incorporated (CC-Bio) or not (Pure CC) with bioactive glass and acquired either before or after 7 days of soaking in simulated body fluid (soaked samples are labeled SBF). Major spectral lines are labeled. Y-axis: intensity (a.u.).

The spectra of both pure CC and CC-Bio evidenced two main peaks related to carbon (C) and oxygen (O), while only the spectrum of CC-Bio showed signals of sodium (Na), calcium (Ca), phosphorus (P), and silicon (Si), confirming the presence of bioactive glass in the composite cryogel. Nitrogen (N), magnesium (Mg), and chloride (Cl) photoelectrons were observed in both cryogels after immersion in SBF for 7 days and were therefore assigned to SBF itself. The O/C ratio for pure cellulose was 0.83 according to the theoretical formula, which was slightly higher than determined for pure CC (0.77). This difference is probably related to C-rich molecular segments (contaminants) adsorbed on the CNF surface. For the CC-Bio sample, the O/C ratio was dramatically reduced (0.58) probably due to the large amount of carbonic species formed on the composite cryogel surface due to the presence of bioactive glass.

The deconvoluted high-resolution XPS spectra for C1s and O1s of pure CC before and after immersion in SBF for 7 days are presented in **Figure S5**. The high-resolution C1s spectrum could be resolved into four, which were related to the individual contributions to the data from different functional groups. The peak at 286.2

eV can be associated to alcohol and ether groups (C-O), while the peak at 287.5 eV associated to acetyl moieties (O-C-O).[6] Peaks at 284.6 eV, related to the non-oxidized alkane-type carbon atoms (-C-C-/-C-H), and at 288.6 eV, attributed to carboxylic functions (O-C=O) from glucuronic acids (hemicelluloses), were also observed.[7] In addition, the spectra showed the presence of impurities associated with carbonated species (*e.g.*, $CaCO_3$ and Na_2CO_3). No significant changes were observed in the pure CC spectra after immersion in SBF (**Figure S5b**). The high-resolution O1s spectra (**Figure S5c**) corroborated with the data observed for the C1s spectrum and revealed the presence of three peaks at 530.8, 532.5, and 534.6 eV, attributed to C=O, C-O-H, and C-O-C, respectively.[8] In the high-resolution O1s spectrum for pure CC after immersion in SBF (**Figure S5d**), a fourth peak at 535.9 eV was required for the best fit, which can be associated to strongly adsorbed water on cryogel surface.

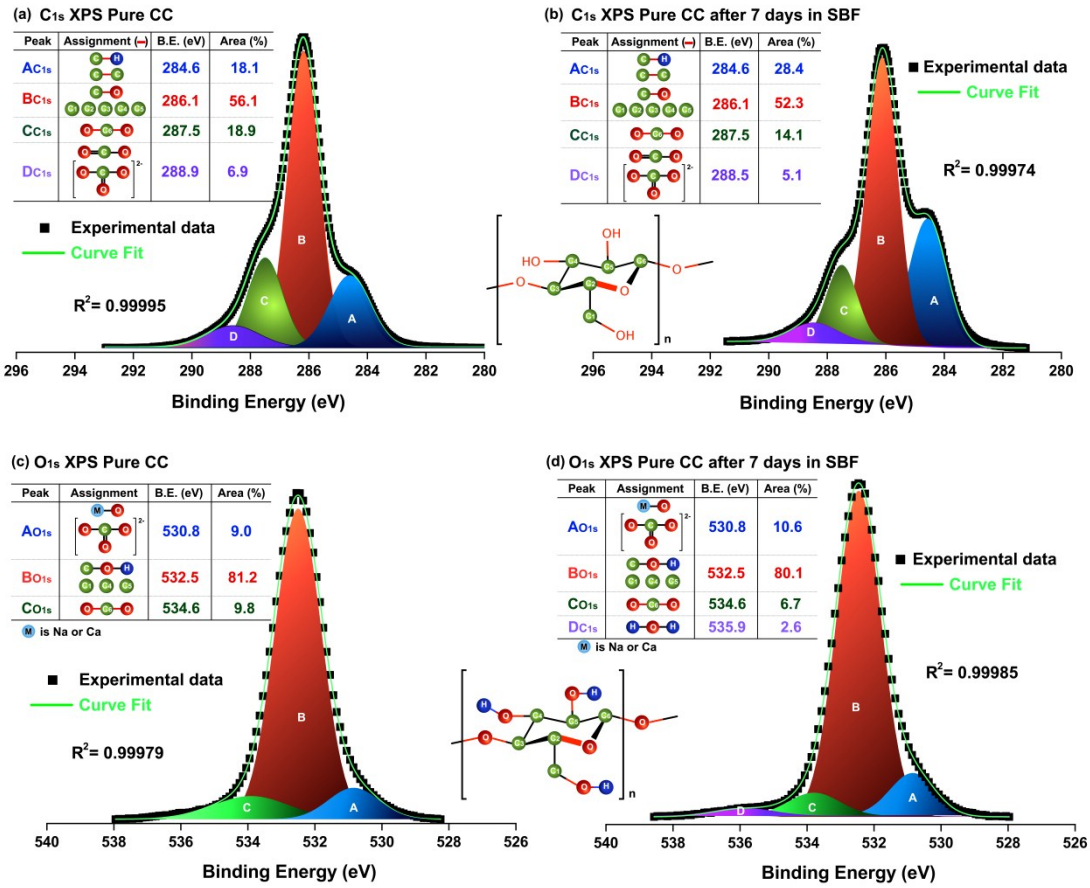

Figure S5. Deconvoluted high-resolution C_{1s} (top; a and b) and O_{1s} (bottom; c and d) X-ray photoelectron spectra of cellulose nanofiber-based cryogels (CC) before (left; a and c) and after (right; b and d) immersion in simulated body fluid (SBF) for 7 days. The assignments of the components from the deconvolution of the C_{1s} high-resolution

spectra were performed according to the proposed numbering for the carbons of the cellulose molecule. Insets: tables displaying the binding energies and percentage areas for each component from the fitting procedure. The broad and narrow scan backgrounds were fit using Shirley backgrounds. All spectra were calibrated to the standard energy of 284.6 eV for the C_{1s} peak.

The C_{1s} high-resolution XPS scans of the CC-Bio (**Figure S6a**) revealed signals consistent with the expected chemical bonding of CNF and changes in the curve profile were observed after immersion in SBF for 7 days (**Figure S6b**). Quantitatively, the fitted area ratios between $C_{C_{1s}}/B_{C_{1s}}$ photopeaks in the pure CC and CC-Bio were 0.64 and 0.34, respectively. This result suggests a chemical interaction between cellulose and the silanol groups (formed during precursor mixture of the gel) present on the surface of bioactive glass particles, *i.e.*, C-O-Si species. The O_{1s} XPS spectrum of CC-Bio (**Figure S6c**) exhibited a different profile from those observed for pure CC in the higher energy region. This portion of the spectrum is related to all contributions of different oxygen associated to silicon such as Si-BO (bridging oxygen) and Si-NBO (non-bridging oxygen) present in bioactive glass particles.[9] A visible shoulder in the spectral portion in lower binding energy at around 530.0 eV (Si-NBO) was also observed. This shoulder disappeared after the immersion in SBF (**Figure S6c**), indicating that the bioactive glass particles have undergone a significant dissolution.[9] According to the mechanism proposed by Hench for glass bioactivity, the first step is associated with rapid ionic exchange between the H_3O^+ of the solution and the modifying ions (Na^+ and Ca^{+2}) present in the glass network.[10] From the point of view of bioactivity (especially for bone tissue engineering), this event is important because it leads to the formation of silanol groups that act as nucleation centers for apatite, which is an important inorganic phase for bone integration[11]. Moreover, several studies have demonstrated that controlled release of biologically active ions from bioactive glasses leads to the up-regulation and activation of important families of genes in osteoprogenitor cells, thus accelerating bone regeneration.[12]

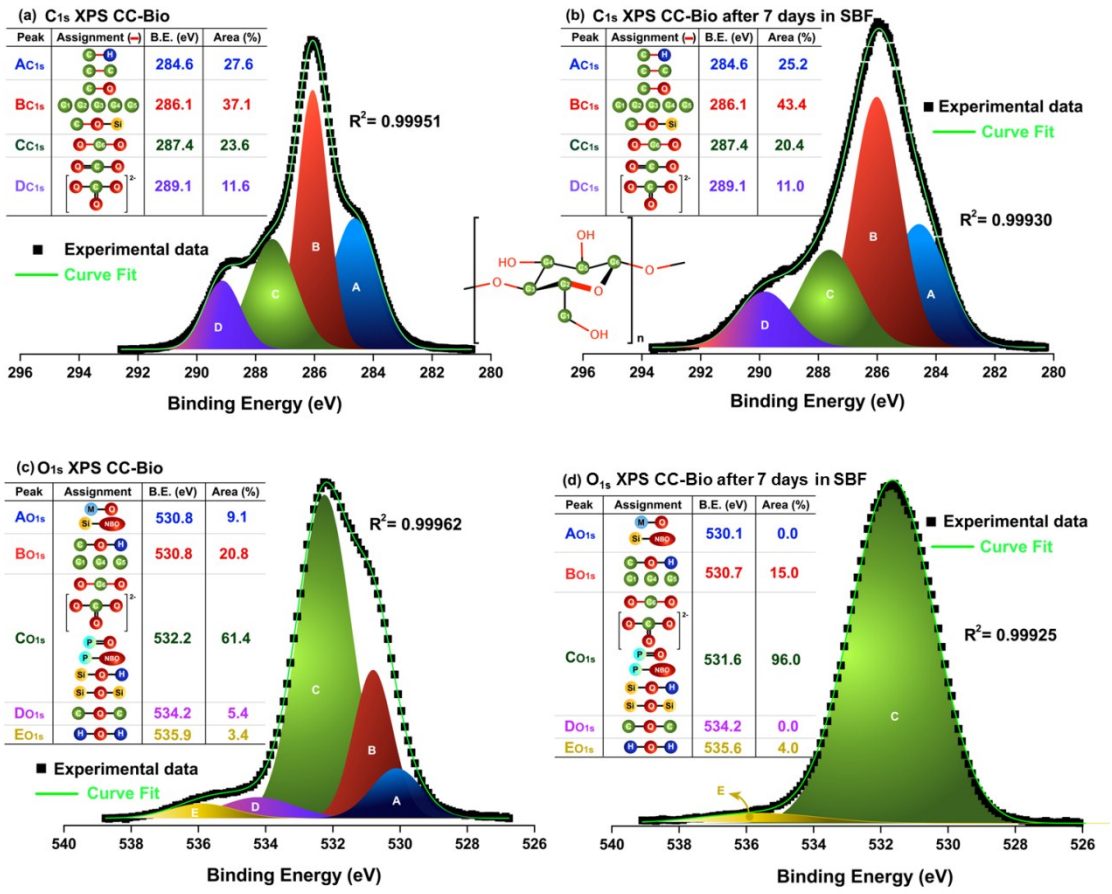

Figure S6. Deconvoluted high-resolution C_{1s} (top; a and b) and O_{1s} (bottom; c and d) X-ray photoelectron spectra of bioactive glass-containing cellulose nanofiber-based cryogels (CC-Bio) before (left; a and c) and after (right; b and d) immersion in simulated body fluid (SBF) for 7 days. The assignments of the components from the deconvolution of the C_{1s} high-resolution spectra were performed according to the proposed numbering for the carbons of the cellulose molecule. Insets: tables displaying the binding energies and percentage areas for each component from the fitting procedure. The broad and narrow scan backgrounds were fit using Shirley backgrounds. All spectra were calibrated to the standard energy of 284.6 eV for the C_{1s} peak.

The deconvoluted spectra Si_{2p}, P_{2p}, and Ca_{2p} of CC-Bio before and after immersion in SBF for 7 days are presented in **Figure S7**. The deconvoluted high-resolution Si_{2p} XPS spectrum (**Figure S7a**) showed a broad distribution of binding energy (99-107 eV) with a maximum at 102.4 eV, which can be attributed to the various Si-Ox species and Si-O-C chemical bonds. In the case of Si-O-C chemical bonds, this result reinforced the assumption that part of the -O-Si-OH (present on the surface of

bioactive glass particles) were converted into O-Si-$C_{Cellulose}$, giving rise to the formation of the cellulose/bioactive glass interface.[13] The Si_{2p} XPS spectra were deconvoluted into two peaks (spin-orbit split doublets) related to the Si $2p_{3/2}$ and Si $2p_{1/2}$ peaks with similar full width at half maxima (FWHM) and binding energy at 102.1 and 103.0 eV, respectively. These spectral features can be related to the overlapping of different signal contributions corresponding to Si-NBO (with 1, 2, 3, and/or 4 non-bridging oxygen) and Si-BO (Si-O-Si) groups related to structural characteristics of the bioactive glass backbone.[14]

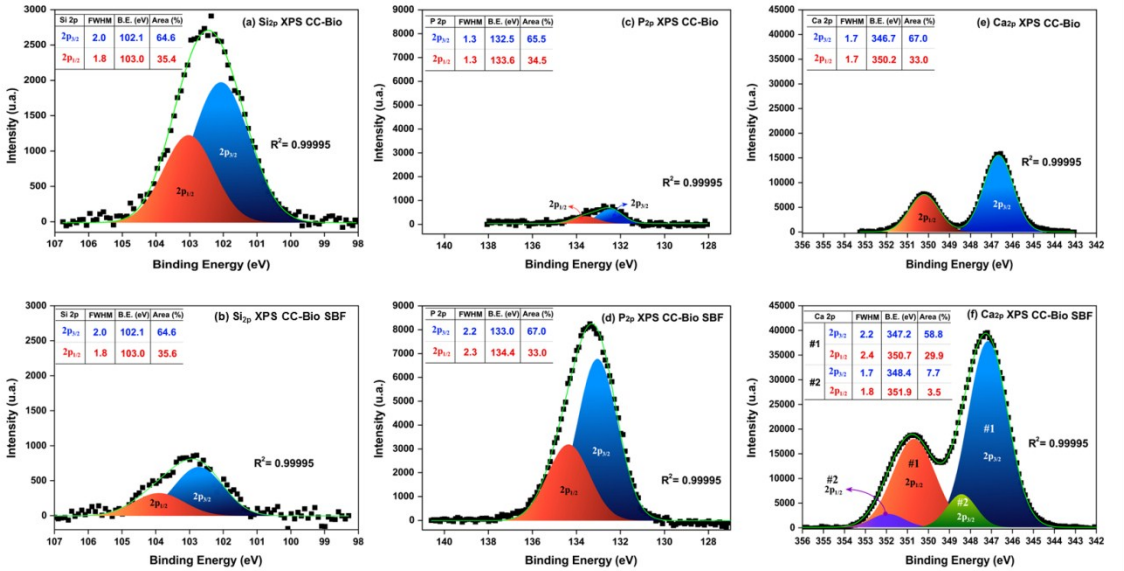

Figure S7. Deconvoluted high-resolution Si_{2p} (left), P_{2p} (center), and Ca_{2p} (right) X-ray photoelectron spectra of bioactive glass-containing cellulose nanofiber-based cryogels (CC-Bio) before (top) and after (bottom) immersion in simulated body fluid (SBF) for 7 days. The high-resolution spectra consist of a spin-orbit split doublet composed of two peaks related to the $2p_{3/2}$ and $2p_{1/2}$ levels. The intensity of the $2p_{1/2}$ peak is constrained by theory to be half the intensity of the $2p_{3/2}$ peak and generally they have similar full width at half maxima (FWHM). Insets: tables displaying the FWHM, binding energies, and percentage areas for each component from the fitting procedure. The broad and narrow scan backgrounds were fit using Shirley backgrounds. All spectra were calibrated to the standard energy of 284.6 eV for the C_{1s} peak.

By comparing the binding energy for Si $2p_{3/2}$ and Si $2p_{1/2}$ peaks for CC-Bio and CC-Bio after 7 days in SBF (**Figure S7a** and **S7b**), a displacement in the binding energies toward higher values was observed, indicating a decrease in the electron density in the chemical environment of silicon. This result suggests that the changes in

the composite cryogel after immersion in SBF promoted not only a partial dissolution of bioglass, but also a polymerization of the silanol groups, leading to formation of silica gel layer (Si–NBO → Si–BO). The formation of a thin layer of silica gel was probably initiated during the preparation of composite cryogel, but intensified in the presence of the SBF. Attenuation of silicon peaks for the high-resolution Si_{2p} XPS spectrum after 7 days immersed in SBF was observed, suggesting that some of the Si species were occluded at least 10 nm deeper into the formed apatite layer on the CC-Bio surface.[15] This assumption was supported by the increase in the intensities relative to P_{2p} and Ca_{2p} in high-resolution XPS spectra after 7 days in SBF (**Figure S7a-e**).

The high-resolution P_{2p} spectrum of CC-Bio (**Figure S7c**) was deconvoluted into two peaks with a spin orbit splitting for $2p_{3/2}$ (132.5 eV) and $2p_{1/2}$ (at 133.6 eV) levels, which refer to the pentavalent phosphorous in PO_4 tetrahedron.[15] The Ca_{2p} XPS spectrum for CC-Bio (**Figure S7d**) was deconvoluted into two peaks for Ca $2p_{3/2}$ and $2p_{1/2}$ (spin-orbit splitting) at 346.7 and 350.2 eV, respectively, which correspond to the calcium specie in the bioactive glass. The deconvolution of Ca_{2p} XPS spectrum for CC-Bio after immersion in SBF (**Figure S7e**) showed four peaks: 347.2 and 348.4 eV, associated with Ca $2p_{3/2}$ level, and 350.7 and 351.9 eV, attributed to the Ca $2p_{1/2}$ contribution. The spin-orbit splitting j (Ca $2p_{3/2}$ - Ca $2p_{1/2}$) was observed at 3.5 eV for both deconvoluted Ca 2p XPS spectra, which can be related to the different calcium compounds. The spin-orbit split doublet presented in lower binding energy can be related to the $CaCO_3$/carbonated apatite, while the chemical environment calcium less shielded (due the ionic character of the bonds) can be attributed to the mixture of calcium phosphates with the predominance of calcium in Ca-deficient hydroxyapatite environment. In fact, the Ca/P ratio decreased from 3.71 (CC-Bio) to 1.60 (CC-Bio after immersion in SBF), making it closely matching to stoichiometric value in phase pure hydroxyapatite (1.66). These results justified the origin of a symmetric and wide peak at 531.6 eV that dominated the core-level XPS spectrum of O_{1s} for CC-Bio after immersion in SBF (**Figure S6d**). The changes in the oxygen chemical environment in the various oxygenates present on the surface of the cryogel were subtle (small variations in the binding energy values), making it difficult to separate components by deconvolution. Furthermore, the increase in the width of P_{2p} and Ca_{2p} XPS spectra for CC-Bio after immersion in SBF confirmed the formation of poorly crystalline calcium phosphate apatite crystals on top of the silica gel layer previously formed by the partial

dissolution of the bioactive glass particles, indicating that the composite cryogel has potential for application in bone repair.[16]

Discussion S5: *In vitro* biocompatibility

Live/dead viability/cytotoxicity assays were performed and the results showed a high number of live cells (green) and a low number of dead cells (red cells) when culturing in CC and CC-Bio (**Figure S8**). MTT viability assay showed (**Figure S8n**) a slight difference when the control was compared with CC and CC-Bio. Despite this difference, both cryogels showed above 80% cell viability, indicating no cytotoxicity.[17] Thus, the results revealed that none of the cryogels significantly affected the metabolic activity and growth of cells and therefore they were cytocompatible. This result is a key parameter since any sign of toxicity represents a risk for the recipient organism[18].

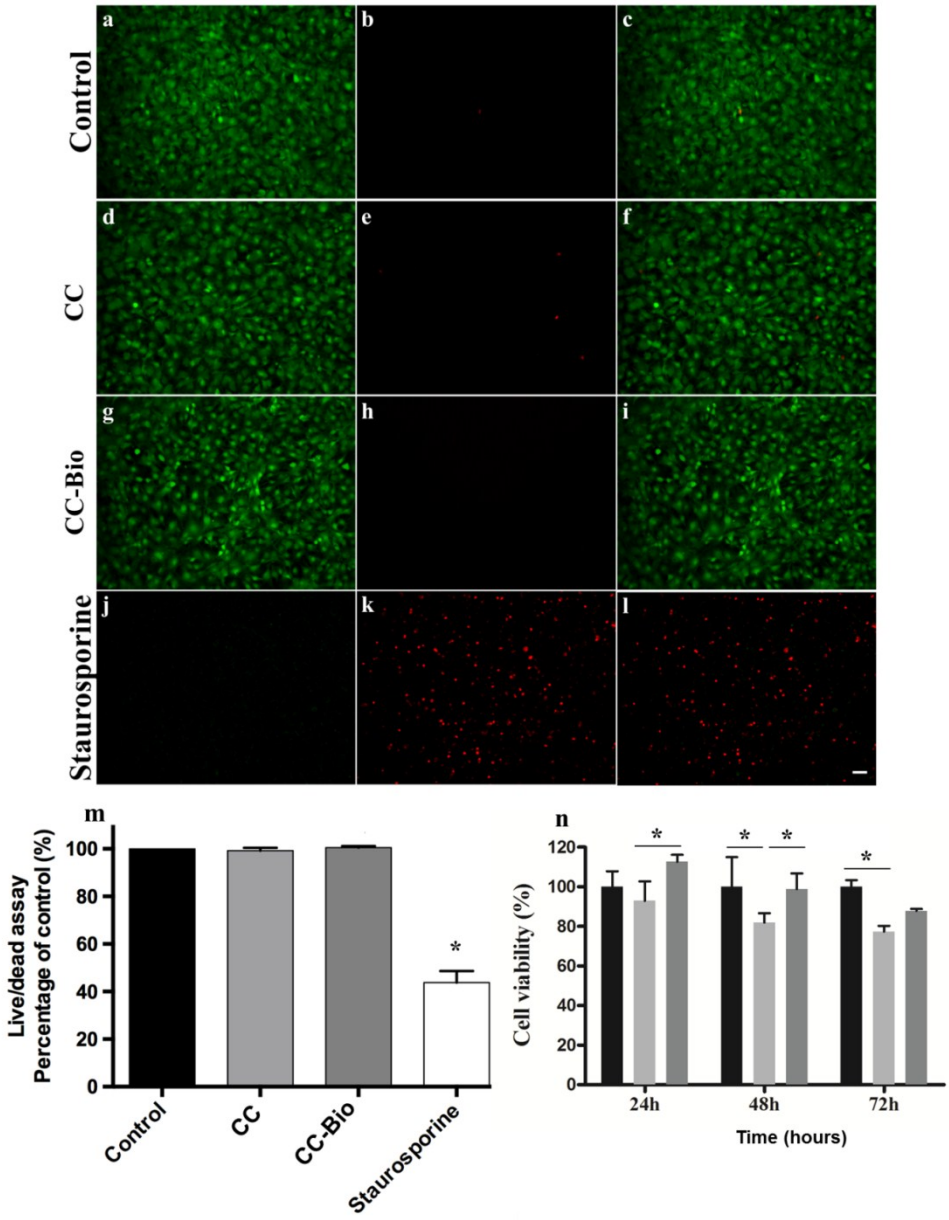

Figure S8. Representative fluorescence images of live/dead staining of MC3T3-E1 cells after culturing for 72 h in the presence of pure (CC; d, e, and f) and bioactive glass-containing (CC-Bio; g, h, and i) cellulose nanofiber-based cryogels. Green/calcein labeling indicates live cells, while red/ethidium bromide labeling marks dead cells. (j, k, l) Staurosporine was used as positive control for cell death, wherea (a, b, c) cells cultured in the absencce of cryogels were used as negative control. Scale bar = 50 μm. (m) Quantification of cell viability. (n) Cell viability determined by MTT reduction assay after 24, 48, and 72 h in culture under indirect contact with CC and CC-Bio. All results are represented by mean values ± standard deviations of triplicates.

Discussion S6: *In vivo* bone formation

The improvement of adhesion of multipotent cells due to formation of hydroxyapatite on the surface of the biomineralized CNF can be explained considering the mechanism through which proteins adsorb onto the scaffold surface. It is well known that scaffold topography and surface chemistry are key factors driving adsorption, in terms of amount and type of proteins immediately after implantation. These proteins serve as binding sites for cell cytoskeleton *via* integrin adhesion, thus forming focal attachments.[19] Depending on the number and the distribution of these attachments, the cells will change their shape. This change is transduced from the cytoskeleton to the nucleus, resulting in alterations in the gene expression and subsequent protein translation.[20]

Discussion S7: Systemic biocompatibility

No significant differences in the concentrations of the biochemical toxicological markers from liver TGO and TGP were obtained in the blood serum of the rat from the control, CC, and CC-Bio groups (**Figure 5a-b**). It indicates that none of the cryogels caused measurable damage to the liver. The same result was observed for creatinine, which is a marker of renal toxicity (**Figure 5c**). These observations were further confirmed by analysis of histological sections of liver and kidney (**Figure 5d-i**), which evidenced neither fibrous tissue nor inflammatory cells as well as showed that the microstructures of both organs were fully preserved. Indeed, our results clearly show that implantation of CC-Bio cryogels caused no harm to metabolic and excretory organs such as liver and kidney. Thus, the incorporation of bioactive glass in the cellulose cryogel maintained its biocompatibility, while promoting a significant enhancement of the biological properties of the implant. The safety of our implants stems from the known biocompatibility of both nanocellulose and bioactive glass. Our findings are first of its kind to demonstrate the systemic compatibility of CNF-based composite cryogels following the analyses of hepatic and renal toxicity markers and histology.

SUPPORTING REFERENCES

1 Y. Habibi, L. A. Lucia and O. J. Rojas, *Chem. Rev.*, 2010, **110**, 3479–3500.

2 C. M. Cowan, Y.-Y. Shi, O. O. Aalami, Y.-F. Chou, C. Mari, R. Thomas, N. Quarto, C. H. Contag, B. Wu and M. T. Longaker, *Nat. Biotechnol.*, 2004, **22**,

560–567.

3 H. Kargarzadeh, J. Huang, N. Lin, I. Ahmad, M. Mariano, A. Dufresne, S. Thomas and A. Gałęski, *Prog. Polym. Sci.*, , DOI:10.1016/j.progpolymsci.2018.07.008.

4 C. G. Otoni, J. S. L. Figueiredo, L. B. Capeletti, M. B. Cardoso, J. S. Bernardes and W. Loh, *ACS Appl. Bio Mater.*, 2019, **2**, 1975–1986.

5 D. Klemm, F. Kramer, S. Moritz, T. Lindström, M. Ankerfors, D. Gray and A. Dorris, *Angew. Chemie Int. Ed.*, 2011, **50**, 5438–5466.

6 H. Hantsche, *Adv. Mater.*, 1993, **5**, 778–778.

7 A. Dufresne, *Mater. Today*, 2013, **16**, 220–227.

8 D. Briggs and G. Beamson, *Anal. Chem.*, 1992, **64**, 1729–1736.

9 M. M. Stevens, *Mater. Today*, 2008, **11**, 18–25.

10 L. Hench and J. Wilson, *Science (80-.).*, 1984, **226**, 630–636.

11 S. Ling, K. Jin, Z. Qin, C. Li, K. Zheng, Y. Zhao, Q. Wang, D. L. Kaplan and M. J. Buehler, *Adv. Mater.*, 2018, **30**, 1802306.

12 J. H. Jordahl, L. Solorio, H. Sun, S. Ramcharan, C. B. Teeple, H. R. Haley, K. J. Lee, T. W. Eyster, G. D. Luker, P. H. Krebsbach and J. Lahann, *Adv. Mater.*, 2018, **30**, 1707196.

13 K. Codling, *Reports Prog. Phys.*, 1973, **36**, 541–624.

14 M. Bohner, *Mater. Today*, 2010, **13**, 24–30.

15 I. Lindau, P. Pianetta, S. Doniach and W. E. Spicier, *Nature*, 1974, **250**, 214–215.

16 Y. Liu, S. Liu, D. Luo, Z. Xue, X. Yang, L. Gu, Y. Zhou and T. Wang, *Adv. Mater.*, 2016, **28**, 8740–8748.

17 N. C. Cady, J. L. Behnke and A. D. Strickland, *Adv. Funct. Mater.*, 2011, **21**, 2506–2514.

18 H. L. Jang, G. Bin Zheng, J. Park, H. D. Kim, H.-R. Baek, H. K. Lee, K. Lee, H. N. Han, C.-K. Lee, N. S. Hwang, J. H. Lee and K. T. Nam, *Adv. Healthc. Mater.*, 2016, **5**, 128–136.

19 Z. Schwartz, C. H. Lohmann, J. Oefinger, L. F. Bonewald, D. D. Dean and B. D. Boyan, *Adv. Dent. Res.*, 1999, **13**, 38–48.

20 B. D. Boyan, E. M. Lotz and Z. Schwartz, *Tissue Eng. Part A*, 2017, **23**, 1479–1489.